Soil Stress Calculation of Bridge Foundation Pit Retaining Pile Based on Improved Terzarghi Method

Jinyu Li*

School of Business Administration, Liaoning Technical University, Huludao, Liaoning 125105, China

*4725201338@stu.lntu.edu.cn

Abstract. The pile-soil stress ratio is a key parameter in pile-soil composite foundations for evaluating bearing capacity, settlement, and reinforcement effect. To reduce significant errors of the traditional Terzaghi method under small deformations, this study introduces an improved approach by revising the slip surface load transfer function. A new stress calculation formula is derived using basic assumptions and equilibrium-deformation coordination equations. Field tests, parameter sensitivity analysis, and comparison with measured data confirm the method's validity. Results show the time-dependent behavior of pile-soil stress ratios and the influence of different parameters. The proposed method better captures non-limit soil arching under small strains, offering a reliable reference for stress analysis in composite foundations.

Keywords: pile-soil composite foundation; pile-soil stress calculation; improved Terzarghi method

1 Introduction

Pile-net composite foundations are widely used in highway, railway and airport projects due to their advantages of small settlement, short construction period and low cost[1]. This system integrates piles, caps, geogrids and inter-pile soil to form a load-bearing structure, where differential settlement between piles and soil leads to stress redistribution, enhancing overall stability and controlling deformation.

Bridge foundations, especially in deep-water environments, are susceptible to erosion-induced soil hollowing, which reduces bearing capacity and threatens structural safety[2]. In pile-net composite foundations, the pile-soil stress ratio—defined as the stress on pile tops relative to that in inter-pile soil—is a key parameter for evaluating bearing performance and settlement[3]. Accurate calculation of this ratio is essential to avoid under-design, excessive differential settlement, or progressive failure. However, classical Terzaghi theory often overestimates load transfer under small differential settlements, leading to significant prediction errors[10]. To address this, the present study proposes an improved Terzaghi-based method by modifying the slip-surface load transfer function and incorporating deformation compatibility. Using

Y. Xu et al. (eds.), *Proceedings of the 2026 5th International Conference on Engineering Management and Information Science (EMIS 2026)*, Advances in Computer Science Research 130,
https://doi.org/10.2991/978-94-6239-652-4_19

field data from a railway project, the variation of inter-pile soil stress and pile-soil stress ratio with fill height is analyzed, and the method is validated against international design codes.The aim is to provide a more reliable calculation tool for engineering practice.

2 Soil Stress Calculation of Bridge Foundation Pit Retaining Pile Based on Improved Terzarghi Method

2.1 Monitoring Arrangement of Bridge Foundation Pit Retaining Pile

The selection of a foundation pit retaining structure depends on excavation depth, geological conditions, site environment, and construction requirements, aiming for safety, feasibility, constructability, and economy. Common retaining structures in China include soil nail walls, bored piles(including interlocking piles), underground continuous walls, concrete-filled piles, and SMW walls[4].For pits deeper than 12 m, bored interlocking piles or underground continuous walls are typically adopted. Interlocking piles usually have a 20 cm overlap; however, when pile length exceeds 30 m, limited vertical precision of equipment can reduce effective interlocking in the lower section, leading to potential deviation.

Foundation pit monitoring serves to verify support design, guide excavation, ensure safety, accumulate experience for design improvement, and enable dynamic control of construction through data analysis, thereby guaranteeing schedule and protecting adjacent structures. In this project, the support system is designed as Safety Level 1.Real-time monitoring was implemented to maintain excavation stability and minimize impact on nearby roads, traffic, and pipelines. Key monitored parameters include wall horizontal displacement, ground settlement, groundwater level, and support axial force, with specific instruments and point arrangements listed in Table 1.

Table 1. Monitoring Items and Instruments

Monitoring items	key	instrumenttation	Number of measurement points
horizontal displacement of wall	○CX	Beijing Aerospace CX-03 Inclination Meter	8
surface subsidence	△C	The DSZ2 Type Precision Leveling Instrument with Microscope	48
water table	◇W	domestic water level gauge	6
supporting shaft force	□ZL	steel wire stress gauge	12

The layout of monitoring points is shown in Figure 1.

Observing wall horizontal displacement versus excavation depth shows that maximum displacement depends on both depth and time. As excavation proceeds, displacement increases and the peak point moves downward, following a parabolic pattern with larger central displacement and smaller ends. After support installation, a slight rebound in displacement occurs.

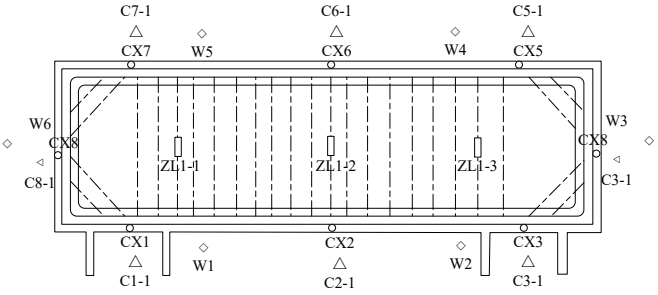

Fig. 1. Plan Layout Diagram of Monitoring Points for Foundation Pit

2.2 Establishment of Soil Stress Change Model for Bridge Foundation Pit Retaining Piles Based on Improved Terzarghi Method

To quantify pile-soil stress variation during consolidation, the classical Terzaghi model requires modification. Its key limitation lies in assuming a limit equilibrium state, which overestimates load transfer under the small deformations typical of low-fill or moderately compressible foundations[10]. For more accurate prediction, this study improves the slip-surface load transfer mechanism. The following assumptions are adopted:(1)fill and foundation soils are homogeneous isotropic elastomers;(2)plane strain condition applies with only vertical deformation;(3)differential pile-soil settlement is smaller than the subgrade's characteristic size, with uniform soil deformation above the foundation;(4)frictional resistance follows an ideal elasto-plastic function relative to shear displacement, with constant shear stiffness G along depth. Based on these, Figure 2 schematically illustrates the improved soil arching model alongside the classical Terzaghi model.

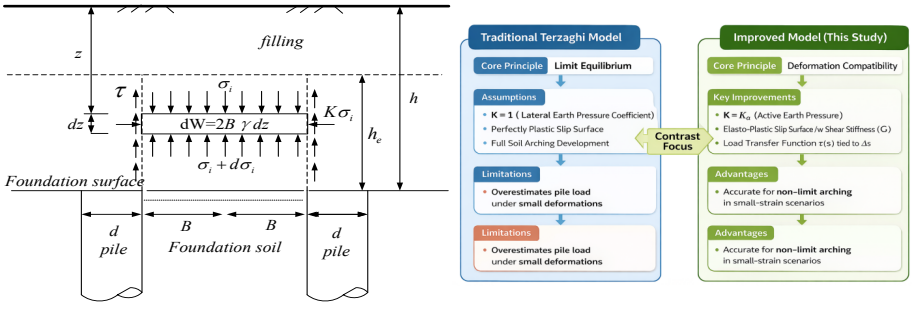

(a) (b)

Fig. 2. Soil arching models: (a) Improved deformation-compatibility model (this study); (b) Classical Terzaghi limit-equilibrium model.

Figure 2(a) presents the improved model developed in this study. Its core innovation lies in modifying the load transfer function on potential slip surfaces. $s\tau s < s_{max}\tau = G \cdot ss \geq s_{max}\tau = \tau_{max}K_aK_a = \tan^2(45° - \varphi/2)K = 1(\tau = \tau_{max})$The model no

longer assumes a fully plastic state but instead controls shear stress through local shear displacement via an ideal elastoplastic relationship (i.e., when, and when), where G denotes shear stiffness. Furthermore, the lateral soil pressure coefficient acting on vertical slip surfaces is more realistically set as the active soil pressure coefficient (where), reflecting stress relaxation in the yielding soil above the pile. In contrast, Figure 2(b) depicts the classical Terzaghi model based on limit equilibrium theory. Its key simplifications include: assuming a lateral soil pressure coefficient and maintaining the entire slip surface in a fully plastic shear state. These assumptions only hold true when differential settlement is sufficiently large to fully utilize the soil arch effect, often significantly overestimating pile loads under small strain conditions.

The proposed model incorporates modifications$\Delta s K_a$—particularly the introduction of an elastic-plastic load transfer function for differential settlement—enabling more accurate description of non-limit earth arch effects under minor deformation conditions. This provides a more reliable theoretical framework for calculating pile-soil stress ratios in common engineering scenarios such as low-fill embankments or moderately low compressibility foundations. The ideal elastic-plastic load transfer function adopted in this improved model is illustrated in Figure 3.

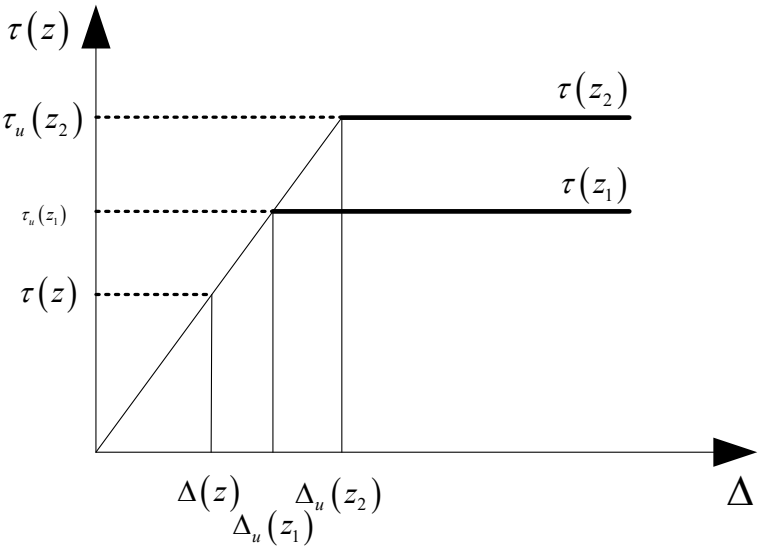

Fig. 3. Elastoplastic models K_S

i.e. (1)

$$K_S = \frac{\tau_u}{\Delta s} = \frac{\tau(z)}{\Delta(z)} \tag{1}$$

Where: τ_u is the ultimate shear strength of soil at the base (kPa); Δs is the differential settlement displacement between pile and soil (m); $\tau(z)$ is the magnitude of shear stress at a given depth on the sliding surface; $\Delta(z)$ is the shear displacement at the same depth on the sliding surface.

Since the soil mass deforms uniformly, it is assumed that the differential settlement between the pile and soil is Δs, and the shear deformation at a depth of z on the sliding surface is

$$\Delta(z) = \beta \Delta s \tag{2}$$

In the formula, the shear deformation coefficient β is a linear function of depth z, with a value of β=0 at the isostatic surface and β=1 at the ground surface. Let the fill height be h and the isostatic surface height be h_e. The geometric relationship yields

$$\beta = (z - h - h_e)/h_e \tag{3}$$

Substituting equation (2) into equation (1), the frictional $\tau(z)$ resistance at a depth of z on the sliding surface can be expressed as

$$\begin{cases} \tau(z) = \begin{cases} 0 & (0 \le z \le h - h_e) \\ \beta \tau_u & (h - h_e \le z \le h) \end{cases} \\ \tau_u = c + fK\sigma_s \end{cases} \tag{4}$$

In the formula: h represents the height of the subgrade (m); c denotes the cohesion of the fill soil (kPa); f is the soil interfacial friction coefficient, $f = tan\varphi$; φ is the internal friction angle of the embankment fill soil; σ_s is the average vertical stress of the soil between piles at the original plane (kPa); K is the lateral soil stress coefficient, which is set to 1 in the Terzarghi method. Under initial stress conditions, the elastic theoretical value of the lateral soil stress coefficient should correspond to the static lateral stress coefficient, typically less than 1. When differential settlement between piles and soil begins, the fill soil above the piles becomes loose, and the soil on both sides tends to actively extrude toward the center. Therefore, the lateral stress acting on the vertical plane should be considered as active soil stress. In this study, the Rankine active soil stress coefficient is adopted $K = K_a = tan^2(45° - \varphi/2)$.

A soil element dz is taken at a depth z above the active door, as shown in Figure 2, and its static equilibrium governing equation is expressed as

$$2B\gamma dz+2B\sigma_s(z)=2B\left(\sigma_s(z)+d\sigma_s(z)\right)+2\tau(z)dz \tag{5}$$

The vertical average stress at a depth of z above the active door is denoted by $\sigma_s(z)$. Substituting equations (2) and (3) into equation (5) and solving the differential equation yields

$$\begin{cases}\sigma_s=\dfrac{2B\gamma h-ch_e}{2B+fKh_e}\\ \sigma_p=\gamma h+\dfrac{2Bh_e}{d}\cdot\dfrac{c+fK\gamma h}{2B+fKh_e}\end{cases} \tag{6}$$

In the formula: σ_s represents the average vertical stress between piles, and σ_p is the average vertical stress at the top of the pile.

The morphology of an asymmetric local erosion pit shows that the upstream erosion pit has a greater slope and depth, while the downstream erosion pit has a smaller slope and depth, presenting an asymmetry. Based on this, the geometric parameters characterizing the asymmetric erosion pit include the upstream erosion depth of the pile S_{d1} , the upstream top width S_{wt1}, the upstream bottom width S_{wb1}, the upstream erosion pit slope β_1, the downstream erosion depth S_{d2}, the downstream top width S_{wt2}, the downstream bottom width S_{wb2}, the downstream erosion pit slope b, and the pile size d.

To validate the proposed asymmetric scour pit stress model, the pile diameter effect was neglected(d=0), and scour pit formation was simulated using the "dead-cell method"[5].The analysis involved two steps: initial ground stress equilibrium, followed by dead-cell simulation of eroded soil within the localized scour pit. The scour pit geometric parameters, along with soil properties(elastic modulus=80 MPa, Poisson's ratio=0.3, effective unit weight=10.4 kN/m³), are listed in Table 2.

Table 2. Parameters of asymmetric scour hole

Independent variable	In situ stress balance	geometric parameter	Pit parameters
S_{wt1}/m	1.35	b/m	1.59
S_{wb1}/m	0.3	$\beta_1/(°)$	39
S_{wt2}/m	2.01	$\beta_2/(°)$	20
S_{wb2}/m	0.27	$\beta_3/(°)$	32
S_{d1}/m	0.837	$(S_{t1}/2)/m$	0.24
S_{d2}/m	0.6324	$(S_{t2}/2)/m$	0.5

The simplified model shows that there are 9 independent variables in the calculation S_{wb1}, S_{wt1}, S_{wb1}, S_{wt1}, S_{d1}, S_{d1}, S_{d2}, S_{wt2}, S_{wb2}, d, b, S_{t1}.To explore the impact of each independent variable on the soil stress in the asymmetric scour pit, this section designs some working conditions around the 9 independent variables and conducts a parameter sensitivity analysis.

Assuming that the soil above the x-plane is an external load (the soil within the local erosion pit that has not been eroded), then below the Ox plane, it is considered a semi-infinite space foundation, and at any depth z below the Ox plane, vertical additional stress components $\Delta\sigma_z$, horizontal additional stress components $\Delta\sigma_x$, and shear stresses.

$$\begin{cases} d\sigma_z = \dfrac{2z^3 dp(x)}{\pi\left(x^2+z^2\right)^2} \\ d\sigma_x = \dfrac{2x^2 z dp(x)}{\pi\left(x^2+z^2\right)^2} \\ \tau_{xz} = \dfrac{2xz^2 dp(x)}{\pi\left(x^2+z^2\right)^2} \end{cases} \tag{7}$$

Therefore, based on the Flamman solution, the additional stress of the surrounding soil under plane strain can be expressed by Equation (7).

The patterns of variation in the horizontal effective stress difference around the pile soil below the Ox plane differ depending on the parameters. The horizontal effective stress of the soil above the Ox plane is calculated using soil pressure theory. As S_{wt1} gradually increases, the horizontal effective stress difference also increases, and the depth of influence also increases. When S_{wt1} remains constant, the horizontal effective stress difference initially increases with depth, then decreases. Under different bottom widths S_{wb1} of the upstream pit of the pile, the soil effective horizontal stress difference exhibits different patterns of variation. As S_{wb1} continuously increases, the horizontal effective stress difference also gradually increases, with the maximum value occurring within the depth range of 1 to 3 meters. An increase in S_{d1} also causes the horizontal effective stress difference to increase; the increasing trend of S_{d1} is particularly noticeable at shallow depths, and the maximum horizontal stress difference can reach 16.96 kPa. Below a depth of 9 meters, the differences between different S_{d1} curves gradually diminish.

In the size sensitivity analysis, a single-variable approach was used for each parameter except pile size, with others held constant. It is noted, however, that the influence of a local scour pit on soil stress in practice results from the synergistic effect of all parameters.

2.3 Optimization of the Soil Stress Algorithm for the Retaining Piles of Bridge Foundation Pit

Based on the displacement status of the retaining structure, soil stress can be categorized into three types:(1)Resting soil stress occurs when the wall remains stationary[6];(2)Active soil stress develops as the wall moves away from the backfill, decreasing to a minimum at soil sliding failure[7];(3)Passive soil stress arises when the wall is pushed toward the fill, increasing to a maximum at ultimate equilibrium[8].Among these, passive stress>resting stress>active stress, and the displacement required to mobilize passive stress is much larger than that for active stress.

For a stationary rigid wall, the soil is in elastic equilibrium, and resting soil stress can be calculated with the following formula:

$$P_0 = \left(\sum \gamma_i h_i + q\right) K_0 \tag{8}$$

In the formula:

P_0 —Calculate the static soil stress intensity (KPa) at the point of interest.

γ_i —Calculate the unit weight (Nk/m³) of the i-th layer of soil above the calculation point

h_i —Thickness of the i-th layer of soil above the calculation point (m)

q —Uniform ground load (kPa)

K_0 —Calculate the static stress coefficient of soil at the point of measurement, determined by the test.

Combined with the similarity theorem, the relationship between the model and prototype ratios of each physical quantity is determined according to the dimensional method, as shown in Table 3.

Table 3. Similar ratio of model tests

physical quantity	symbol	dimension	Model/Prototype
length	L	L	I/N
area	A	L2	I/N2
volume	V	L3	I/N3
quality	M	M	I/N3
density	ρ	ML-3	I/I
stress	σ	ML-1T-2	I/I
meet an emergency	ε	I	I/I
displacement	δ	L	I/N
uniform force	q	ML-1T-2	I/I
concentrated force	P	MLT-2	I/N2
modulus of elasticity	E	ML-1T-2	I/I

The experimental soil materials comprised silty soft soils identical to the in-situ foundation, with cement-soil mixtures and steel prepared per design specifica-

tions.Vertical drainage systems matched the project's plastic drainage boards, enhancing the practical relevance of results[9].

Field measurements show that pile-soil stress exhibits clear time-dependent characteristics, akin to consolidation settlement, rather than remaining constant. In low-fill or moderately compressible foundations, differential pile-soil deformation is typically small;here the traditional Terzaghi method yields significant errors[10].To improve accuracy, this study extends the Terzaghi model by assuming uniform fill deformation under small strains, adopting an equivalent-stiffness ideal elastoplastic function for interfacial friction, and combining equilibrium and deformation-compatibility equations to derive theoretical solutions for pile-soil stress and soil-arch height. The model further analyzes parameter influences, membrane-effect development, time-varying stress-ratio behavior, and is validated against field data.

Parameter analysis indicates that soil vertical effective stress rises with scour-pit size, with deeper influence zones for larger pits. Control-variable sensitivity analysis shows that single-parameter changes in upstream/downstream pit top/bottom widths cause minor variation in vertical stress, whereas differential scour depth across the pile sides exerts a pronounced effect.

Asymmetric scour pits induce differences in horizontal stress between upstream and downstream soils. Sensitivity studies reveal that horizontal effective-stress difference first increases then decreases with depth, approaching zero beyond 10 m. Under fixed scour-pit geometry, increasing pile size reduces the vertical effective-stress rate at a given depth, with the difference peaking then declining as depth grows[11][12].Horizontal stress difference across the pile also decreases with larger pile size, showing strong influence within 3 m depth but diminishing below 3 m, and nearing zero at 9 m.

3 Performance Testing

3.1 Overview of Test Section and Geological Conditions

The experimental soils replicated the in-situ silty soft foundation, with cement-soil and steel materials prepared as specified. Vertical drainage matched the project's plastic drainage boards, improving result relevance[9]. Field data confirm that pile-soil stress varies with time, similar to consolidation settlement. In low-fill or moderately compressible foundations, small differential deformation leads to significant error when using the traditional Terzaghi method[10]. This study therefore improves the Terzaghi model by assuming uniform fill deformation under small strains, adopting an equivalent-stiffness ideal elastoplastic interfacial friction law, and combining equilibrium and deformation-compatibility equations to solve for pile-soil stress and soil-arch height. The model also examines parameter influences, membrane-effect development, time-varying stress-ratio behavior, and is validated with field measurements.

Parameter analysis shows that vertical effective stress increases with scour-pit size, influencing deeper zones for larger pits. Sensitivity analysis indicates that varying only the top/bottom widths of upstream/downstream pits causes minor changes in

vertical stress, whereas differential scour depth across the pile sides has a significant effect. Asymmetric scour pits induce horizontal stress differences between upstream and downstream soils; this difference first rises then falls with depth, approaching zero beyond 10 m. With fixed scour-pit geometry, larger pile sizes reduce the vertical effective-stress rate at a given depth, the difference peaking then declining with depth[11][12].Horizontal stress difference across the pile also decreases with larger pile size, strongly influencing the upper 3 m, diminishing below 3 m, and nearing zero at 9 m.

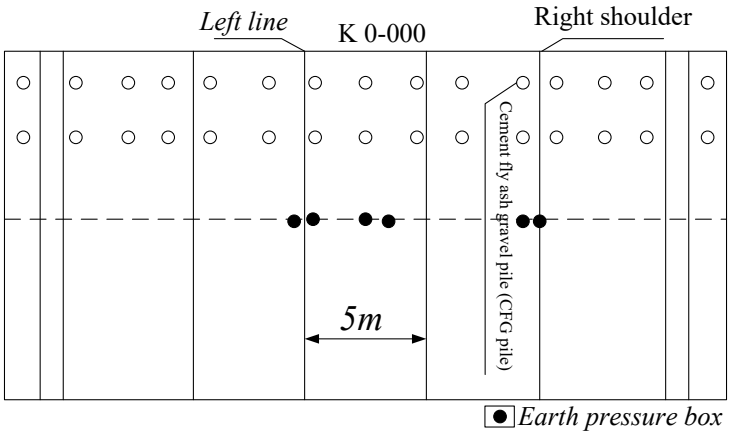

Fig. 4. Layout Plan of Measurement Points for CFG Pile-Net Composite Structure

Two units per group are arranged: one at the pile top and one in the inter-pile soil, totaling six units as shown in Figure 4.

The current field validation is based on a specific geological and structural condition. To further verify the robustness and generalizability of the improved method, future work plans to apply and test the model in scenarios with different soil types(e.g., soft clay, sandy soil)and other foundational support structures(e.g., diaphragm walls).

3.2 Results and Analysis

The case study data originates from Wang Wei's field measurements at the DK559+650 section of the Liunan Line. The foundation consists of expansive soil and soft clay, with limestone underlying it. The soil's compressibility coefficient ranges from 0.091 to 0.152 MPa-1, classifying it as a moderately low-compressibility foundation. The CFG pile and geogrid treatment was implemented, featuring 6-meter-long piles with 0.5-meter diameter and 1.8-meter spacing, without pile caps. Calculation parameters are detailed in Table 4.

Table 4. Calculation parameters of Liu-nan railway (section DK559+650)

Material type	Calculation parameters	Material type	Calculation parameters
Embankment fill	$h = 10.3m$	Embankment fill	$c = 15kPa$
Embankment fill	$\varphi = 30°$	Embankment fill	$E_s = 20MPa$
Embankment fill	$E_0 = 15MPa$	Embankment fill	$\gamma = 19.8\,KN/m^3$
pile	$d = 0.5m$	pile	$B = 0.65m$
Geogrid	$E_g = 160\,KN/m$		

The test results and calculation results are shown in Figure 5.

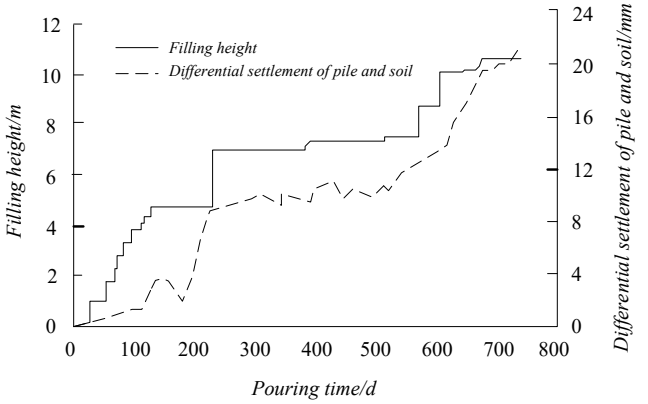

Fig. 5. Filling height and differential settlement of pile and soil

As shown in Figure 5, pile-soil differential settlement varies with fill height and time. The inter-pile soil stress calculated by the improved method agrees better with measurements than the Terzaghi method. The pile-soil stress ratio shows clear time-dependence: rising quickly early on, then stabilizing, and correlating with differential settlement. At 200 and 600 days in Figure 5, abrupt changes occur due to sudden fill increments, which first decrease then increase the ratio—consistent with prior analysis. After stabilization, calculated and measured values align well, confirming the method's applicability to general pile-net composite foundations.

4 Conclusion

(1)To address the limitations of the Terzaghi soil arch model in small-deformation analysis, this study improves the method by revising the slip-surface load transfer function. A pile-soil stress calculation formula incorporating the membrane effect is derived, revealing the relationship between soil arching and differential settlement. The improved method outperforms Terzaghi's approach, showing better agreement

with measured stress ratios and inter-pile stresses, and is more suitable for evaluating non-limit soil arch effects in small-strain conditions.

(2)As differential settlement increases, soil-arch height growth initially accelerates then decelerates, while the soil-arch ratio follows a hyperbolic reduction, eventually approaching the Terzaghi limit ratio—consistent with test results. The pile-soil stress ratio rises with differential settlement and increases with higher fill cohesion and optimal pile spacing. Greater fill height raises the soil-arch ratio but reduces arching intensity, lowering the stress ratio. The tensile membrane effect becomes fully effective only after differential settlement reaches a threshold.

(3)The pile-soil stress ratio exhibits clear time-dependence: rising rapidly during early filling, then stabilizing. Compared to conventional methods, this approach can predict stress variation with settlement at different construction stages. A current limitation is the need for measured differential settlement data, which will be addressed in future research.

(4)Based on the Terzaghi method, a calculation framework is established that accounts for non-limit soil arching under small deformations and relates arching to differential settlement. It provides expressions for soil-arch height and pile-soil stress, enabling analysis of their time-varying characteristics.

(5)The model is currently validated for homogeneous soil, small deformations, and static loading. Future work should extend its application to heterogeneous strata, large deformations, and dynamic loads(e.g., seismic or traffic cycles), and test it across varied geological conditions and support types to enhance reliability.

(6)The improved method has strong potential for engineering practice. Integrated with IoT sensor systems, it can support real-time monitoring and early warning during construction, enabling dynamic design and risk control. To promote adoption, the algorithm could be embedded in geotechnical software or compiled into design guidelines, and disseminated through training and pilot projects.

References

1. Su Yanhuan. (2023). Research on the impact of pile-net composite foundation on highway soft soil foundation settlement. China New Technology and Products, (08), 89-91.
2. Li Juntang, Qin Shunquan & Zhang Ruixia. (2020). Development and Prospects of Deep Water Foundation for Bridges. Bridge Construction, 50(03), 17-24.
3. Yu Genshe, Shang Yonghui & Xu Linrong. (2024). High-strength grating pile-net foundation load transfer pile-soil stress characteristics. Journal of Jilin University (Engineering Edition), 54(06), 1730-1737.
4. Shi Xubo, Feng Shikai & Li Zhuo. (2024). Mechanical Properties and Deformation of Deep Foundation Pit Retaining Structures. Groundwater, 46(03), 317-319.
5. Wang Zengliang, Zhou Hang, Ding Xuanming, Wu Daifeng, Cai Ruyi & Xiao Zhiwei. (2021). Simplified model for soil stress calculation under three-dimensional asymmetric local scour pit conditions in pile foundations. Journal of Civil and Environmental Engineering (Chinese and English), 43(05), 45-57.
6. Rui, R., Xia, R. J., Han, J., Ye, Y. Q., Miao, X., & Elabd, M. Rui, R., Xia, R. J., Han, J., Ye, Y. Q., Miao, X., & Elabd, M. (2024). Experimental investigations of lateral earth

pressures behind rigid retaining walls under different displacement modes. Acta Geotechnica, 19(5), 2545-2562.
7. Lyu, P., Luo, Q., Wang, T., Connolly, D. P., & Ye, Q. Lyu, P., Luo, Q., Wang, T., Connolly, D. P., & Ye, Q. (2025). Serviceability of railway slab track foundations with retaining walls under train loading. International Journal of Rail Transportation, 13(1), 23-48.
8. Liu, G., Dang, F., Wang, X., Li, Y., & Zheng, W.Liu, G., Dang, F., Wang, X., Li, Y., & Zheng, W. (2025). Calculation and analysis of passive earth pressure under ultimate stress conditions. Scientific Reports, 15(1), 38378.
9. Khan, S. A., Karray, M., & Paultre, P. Khan, S. A., Karray, M., & Paultre, P. (2023). Seismic behavior of retaining walls: a critical review of analytical and field performance studies. Geotechnics, 4(1), 54-77.
10. Liu Wei, Gao Yuan, Zhou Yitao, Gao Junming & Du Xigang. (2012). Improved algorithm for soil arch effect in pile-supported embankments based on the Terzaghi method. Hebei Industrial Science and Technology, 29(02), 95-97.
11. Al-Atroush, M. E., Hefny, A. M., & Sorour, T. M. Al-Atroush, M. E., Hefny, A. M., & Sorour, T. M. (2022). Modified Meyerhof approach for forecasting reliable ultimate capacity of the large diameter bored piles. scientific reports, 12(1), 8541.
12. Lin, C., & Wu, R.Lin, C., & Wu, R. (2019). Evaluation of vertical effective stress and pile lateral capacities considering scour-hole dimensions. Canadian Geotechnical Journal, 56(1), 135-143.